View Online

A facile synthesis of anatase TiO_2 nanosheets-based hierarchical spheres with over 90% {001} facets for dye-sensitized solar cells†

Weiguang Yang,[ab] Jianming Li,[a] Yali Wang,[b] Feng Zhu,[a] Weimin Shi,[b] Farong Wan[c] and Dongsheng Xu*[a]

Received 17th August 2010, Accepted 19th November 2010
DOI: 10.1039/c0cc03312j

Published on 06 December 2010 on http://pubs.rsc.org | doi:10.1039/C0CC03312J
Downloaded by Universitat Basel on 11 February 2011

Anatase TiO_2 nanosheets-based hierarchical spheres with over 90% {001} facets synthesized *via* a diethylene glycol–solvothermal route were used as photoanodes of dye-sensitized solar cells, which generated an energy conversion efficiency of 7.51%.

Dye-sensitized solar cells (DSSCs), which emerged as a new generation photovoltaic device, have been studied extensively because of their high efficiency, low cost and facile fabrication process.[1] The heart of the DSSC system is a wide bandgap semiconductor nanoparticle film that provides a large surface area for the adsorption of light-harvesting molecules. Because attached to the surface of the nanocrystalline film is a monolayer of the charge transfer dye, an increase of the surface roughness factor of the nanocrystalline film is very necessary to meet the requirement of efficient harvesting of sunlight. Classically, thick mesoporous wide-band gap oxide semiconductor films with an enormous internal surface area, typically a thousand times larger than that of bulk films, were used as the photoelectrode of DSSCs.[2] However, the high surface area of a nanocrystalline film should bring about many opportunities for the recombination of photoinjected electrons and the oxidized dye and/or the electron acceptors in the electrolyte. In addition, since the sensitizers (typically, N3 or N719) have low absorption efficiency in the red region, large particles are incorporated into the film to enhance the photoresponse to red light by means of light scattering effects. However, the reduction of surface area counteracts the enhancement effect of light scattering on the optical absorption. Moreover, improving the absorption of red and near-infrared light through thickening the nanoparticle film to increase its optical density is limited by the electron diffusion length through the nanoparticle network.[3]

To balance the light scattering and surface area effects, hierarchically mesoporous microspheres, which are comprised of polydisperse aggregates consisting of nanosized crystallites, have been studied.[4–6] The mesoporous microspheres are submicrometre-sized and, thus, can function as efficient light scatters, while the nanocrystallites provide the films with the necessary mesoporous structure and large internal surface area. However, a decrease of the electron diffusion length arose by large amounts of electron traps while keeping high surface area is still a big problem for those mesoporous microspheres assembled by nanosized crystallites. Herein, we report a facile and nontoxic solvothermal route of preparation of anatase TiO_2 nanosheets-based hierarchical spheres (ATNHSs) as the photoanodes in DSSC for the improvement of energy conversion efficiency. Although several studies by research groups worldwide have developed new routes to prepare more anatase TiO_2 sheets with exposed {001} facets,[7] the synthesis of 3D hierarchitectures self-assembled with sheetlike anatase TiO_2 as building blocks is up to date extremely sparse.[8] Compared to the mesoporous spheres consisting of nanosized crystallites, we proposed that the nanosheet-like architectures can effectively minimize the grain interface effect, and the anatase (001) surfaces with high surface energy have strong ability to dissociatively absorb (COOH) group.[9] As a result, an overall energy conversion efficiency up to 7.51% has been achieved, indicating a 43% increase compared to the standard Degussa P25 photoanode (5.26%).

ATNHSs with dominantly exposed {001} facets have been synthesized by a diethylene glycol (DEG)–solvothermal method, in which TiF_4 was used as a Ti precursor. In a typical experiment, 5 mL of acetic acid was added in a 0.01–0.03 M TiF_4–DEG solution under magnetic stirring for 3 h at room temperature, and then transferred to a Teflon-lined stainless steel autoclave of 50 mL capacity and heated for 8 h at 180 °C with a heating rate of 1 °C min^{-1}. Fig. 1 shows the scanning electron microscopy (SEM) images of the products prepared at different TiF_4 concentrations, indicating a hierarchical structure with numerous randomly arranged TiO_2 nanosheets. The as-prepared ATNHSs

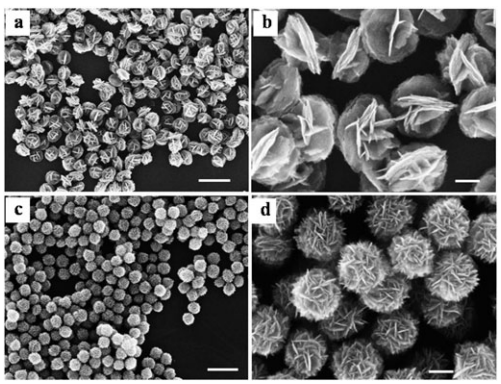

Fig. 1 SEM images of the hierarchically structured TiO_2 nanosheets prepared at different TiF_4 concentrations: (a and b) 10 mM; (c and d) 30 mM. Scale bars: (a, c) 500 nm; (b, d) 100 nm.

[a] *Beijing National Laboratory for Molecular Sciences, State Kay Laboratory for Structural Chemistry of Unstable and Stable Species, College of Chemistry and Molecular Engineering, Peking University, Beijing 100871, China. E-mail: dsxu@pku.edu.cn; Fax: +86 10-62760360; Tel: +86 10-62753580*
[b] *School of Materials Science and Engineering, Shanghai University, Shanghai 200444, China*
[c] *Beijing Key Lab of Advanced Energy Material and Technology, Department of Materials Physics and Chemistry, University of Science and Technology Beijing, Beijing100085, China*
† Electronic supplementary information (ESI) available: Experimental details and figures. See DOI: 10.1039/c0cc03312j

View Online

Published on 06 December 2010 on http://pubs.rsc.org | doi:10.1039/C0CC03312J
Downloaded by Universitat Basel on 11 February 2011

prepared at a TiF_4 concentration of 10 mM are quite uniform with an average diameter of 250 nm (Fig. 1a). The higher magnification micrograph shows that the TiO_2 nanosheets in the hierarchical structures are 7 nm in thickness and 30–180 nm in diameter (Fig. 1b). With increasing the TiF_4 concentration to 30 mM (Fig. 1c and d), the average diameter of the obtained microspheres decreases from 250 nm to 200 nm and the amounts of constituent nanosheets tend to increase, while the thickness of the constituent nanosheets remains about 7 nm.

Fig. 2a displays the X-ray diffraction (XRD) pattern of the as-prepared ATNHSs with an average diameter of 200 nm, giving a pure anatase TiO_2 phase. The relative intensities of the (200) and (004) reflections represent the *a* and *c* axes, respectively. The (200) reflection of the as-synthesized product is significantly more intense and sharper than both the (004) and (101) peaks, indicating a domain crystalline growth along the *a* axis. Fig. 2b shows the nitrogen adsorption–desorption isotherm of the ATNHSs. The isotherm displays the typical type IV curve with a H3 hysteresis according to the IUPAC classification, which is usually ascribed to slit-like mesopores formed by sheet-like particles.[10] The Barrett–Joyner–Halenda (BJH) pore size distribution (Fig. 4b) obtained from the isotherm indicates that the BET specific surface area is $\sim$63.5 $m^2\ g^{-1}$ and the ATNHS sample contains two types of the pores. The first type of pores may be ascribed to a smaller portion of mesopores (about 2.5 nm) attributed to the parallel assembly of the nanosheets. The second type comprises a majority of the slit-like mesopores (about 17.9 nm) which resulted from randomly assembled nanosheets. Besides, the voids formed by interaggregated ATNHSs may also contribute to the second type of pores.

The microstructures of the ATNHSs were further characterized by transmission electron microscopy (TEM). Fig. 3a reveals that the entire structure of the architecture is built from several dozens of self-organized TiO_2 nanosheets. A representative higher-resolution TEM image of a single

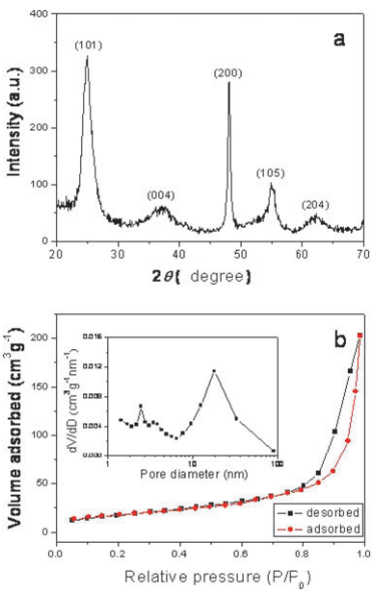

Fig. 2 (a) XRD pattern and (b) nitrogen adsorption–desorption isotherm and Barret–Joyner–Halenda (BJH) pore size distribution plot (inset) of the as-prepared sample prepared at the TiF_4 concentration of 30 mM.

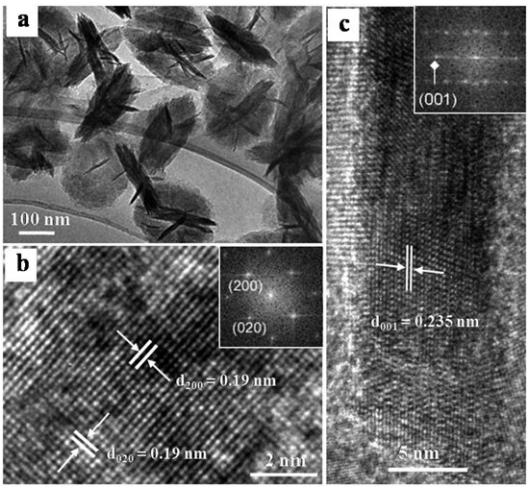

Fig. 3 (a) Low-magnification TEM and (b and c) high-resolution TEM images of the ATNHSs prepared at a TiF_4 concentration of 30 mM. The insets show the corresponding FFT patterns.

nanosheet is given in Fig. 3b. Two sets of the lattices with an equal fringe spacing of 0.19 nm and an interfacial angle of 90° are in well agreement with the (200) and (020) planes of anatase TiO_2.[7a] The corresponding fast Fourier transform (FFT) pattern (the inset in Fig. 3b) can be indexed to diffraction spots of the [001] zone. Furthermore, the HRTEM image from the vertical nanosheet (Fig. 3c) shows that the lattice fringes spacing of 0.235 nm parallel to the top and bottom facets are assigned to (001) planes of anatase TiO_2. On the basis of the above structural information, the percentage of exposed {001} facets of the ATNHSs can be estimated to be over 90%.

The formation mechanism of such a nanosheet-based hierarchical structure could be understood by the capping effect of fluorine ions on the exposed {001} facets. Generally, the synergistic functions of fluorine ions can markedly reduce the surface energy of the {001} facets to a level lower than that of {101} facets.[7a] The emerging high-energy (001) facets are most effectively stabilized by fluorine ions formed in the hydrolysis reaction of TiF_4, which significantly retards their growth along the [001] direction. In addition, we found that in a control experiment, with the replacement of DEG by triethylene glycol, no nanosheet-like structure was observed (Fig. S1, ESI†). The unsaturated Ti^{4+} cations on the (001) and (101) surfaces are inclined to be coordinatively bound to DEG or deprotonated DEG molecules.[11] Therefore, it is hypothesized that DEG could also acts as a protective capping agent and the growth rate along the (001) direction relative to the (101) direction is further retarded.

DSSCs consisting of TiO_2 films with the ATNHSs were tested by measuring the current–voltage behaviour under illumination with a power density of 100 mW cm^{-2}. For comparison, the TiO_2 photoanodes made of commercial Degussa P25 TiO_2 nanoparticles were also investigated. Fig. 4a shows the typical current density *versus* voltage curves of the ATNHSs and P25 photoanodes. It can be seen that the TiO_2 photoanodes made from the ATNHSs show a J_{sc} of 17.9 mA cm^{-2} and a V_{oc} of 0.65 V with the energy conversion efficiency (η) of 7.51%, whereas the photoanodes made from P25 nanoparticles give a J_{sc} of 11.6 mA cm^{-2} and a

 This journal is © The Royal Society of Chemistry 2011

View Online

Published on 06 December 2010 on http://pubs.rsc.org | doi:10.1039/C0CC03312J
Downloaded by Universitat Basel on 11 February 2011

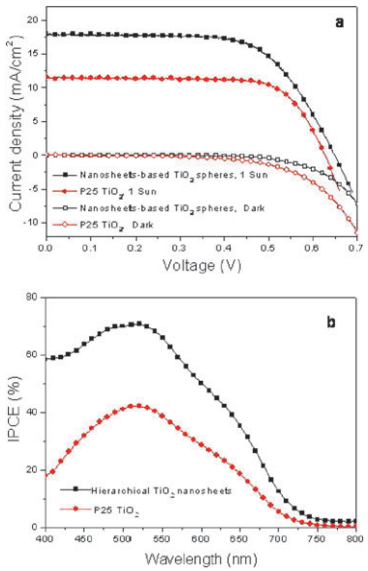

Fig. 4 (a) Comparison of the current–voltage characteristics of DSSCs based on the ATNHSs and P25 TiO_2. (b) IPCE spectra as a function of wavelength in the dye-sensitized ATNHSs and P25 films with the similar thickness (about 14 μm).

V_{oc} of 0.63 V with a η of 5.26%, indicating 54% and 43% increases in J_{sc} and η compared to the P25 photoanodes of the similar thickness, respectively. Meanwhile, a decrease of the dark current demonstrated that the nanosheet-like architecture can effectively minimize the grain interface effect and reduce the electron loss. To analyze in more detail the enhanced cell performance, incident monochromatic photo-to-electron conversion efficiency (IPCE) measurements were conducted. Fig. 4b shows the IPCE as a function of wavelength measured at short circuit. The IPCE is determined by the light absorption efficiency of the dye, the quantum yield of electron injection, and the efficiency of collecting the injected electrons at the conducting glass substrate,[12] which is strongly affected by the morphology and surface area of the photoelectrode.[13] Compared with the P25 TiO_2 film, the film of the ATNHSs had a higher IPCE from 400 nm to 750 nm wavelength ranges. At the maximum value of the IPCE spectra at 520 nm, the IPCE of the film of the ATNHSs was approximately 67% higher than that of the P25 TiO_2 film.

The great improvement in the J_{sc} and η of the ATNHSs can be attributed to the following outstanding features: (i) the anatase (001) surfaces with high surface energy have strong ability to dissociatively absorb (COOH) group.[9] During this process, the carbonyl O atom binds to 5-fold Ti (Ti_{5C}) on the (001) surfaces, while the hydroxy H is transferred to O_{2C}.[14] This can increase the electronic coupling between the sensitizer and the TiO_2 semiconductor and favor electron injection from the excited state of the sensitizer into the TiO_2 conduction band;[15] (ii) the ATNHSs have high surface area, which is essential to increase dye loading, and meanwhile, the submicrometre-sized TiO_2 spheres can promote the light harvesting of the N719 dye within the photoanodes due to the light scattering effect (Fig. S2, ESI†); (iii) the unique hierarchical structure built from nanosheets with large particle sizes can effectively minimize the grain interface effect and thus reduce the electron loss.

In summary, we have developed a facile solvothermal method for the synthesis of ATNHSs with dominantly exposed {001} facets. The obtained hierarchical TiO_2 spheres consist of ultrathin anatase nanosheets (~7 nm in thickness and 30–180 nm in lateral size), with diameters of 200–250 nm and a specific surface area of ~63 $m^2\ g^{-1}$. Inspired by the unique structure, the photoanodes of DSSC made from these hierarchical spheres exhibit great improvement in J_{sc} and η. We expect that such ATNHSs will have a good potential for the applications in energy conversion and catalysis, because their dominantly exposed {001} surfaces with high surface energy and high surface area provide multiple benefits.

This work was supported by NSFC (Grant No. 50821061) and MSTC (MSBRDP, Grant Nos. 2006CB806102, 2007CB936201).

Notes and references

1 (*a*) B. O'Regan and M. Grätzel, *Nature*, 1991, **353**, 737; (*b*) M. Grätzel, *Nature*, 2001, **414**, 338.
2 (*a*) M. Zukalova, A. Zukal, L. Kavan, M. K. Nazeeruddin, P. Liska and M. Grätzel, *Nano Lett.*, 2005, **5**, 1789; (*b*) M. K. Nazeeruddin, P. Pechy, T. Renouard, S. M. Zakeeruddin, R. H. Baker, P. Comte, P. Liska, L. Cevey, E. Costa, V. Shklover, L. Spiccia, G. B. Deacon, C. A. Bignozzi and M. Grätzel, *J. Am. Chem. Soc.*, 2001, **123**, 1613.
3 S. Nishimura, N. Abrams, B. A. Lewis, L. I. Halaoui, T. E. Mallouk, K. D. Benkstein, J. van de Lagemaat and A. J. Frank, *J. Am. Chem. Soc.*, 2003, **125**, 6306.
4 Q. F. Zhang, T. P. Chou, B. R. Russo, S. A. Jenekhe and G. Z. Cao, *Angew. Chem., Int. Ed.*, 2008, **47**, 2402.
5 D. Chen, F. Huang, Y.-B. Cheng and R. A. Caruso, *Adv. Mater.*, 2009, **21**, 2206.
6 W. G. Yang, F. R. Wan, Q. W. Chen, J. J. Li and D. S. Xu, *J. Mater. Chem.*, 2010, **20**, 2870.
7 (*a*) H. G. Yang, C. H. Sun, S. Z. Qiao, J. Zou, G. Liu, S. C. Smith, H. M. Cheng and G. Q. Lu, *Nature*, 2008, **453**, 638; (*b*) B. H. Wu, G. Y. Guo, N. F. Zheng, Z. X. Xie and G. D. Stucky, *J. Am. Chem. Soc.*, 2008, **130**, 17563; (*c*) D. Q. Zhang, G. S. Li, X. F. Yang and J. C. Yu, *Chem. Commun.*, 2009, 4381–4383; (*d*) Y. Q. Dai, C. M. Cobley, J. Zeng, Y. M. Sun and Y. N. Xia, *Nano Lett.*, 2009, **9**, 2455; (*e*) M. Liu, L. Y. Piao, L. Zhao, S. T. Ju, Z. J. Yan, T. He, C. L. Zhou and W. J. Wang, *Chem. Commun.*, 2010, **46**, 1664.
8 J. S. Chen, Y. L. Tan, C. M. Li, Y. L. Cheah, D. Luan, S. Madhavi, F. Y. C. Boey, L. A. Archer and X. W. Lou, *J. Am. Chem. Soc.*, 2010, **132**, 6124.
9 (*a*) A. Vittadini, M. Casarin and A. Selloni, *Theor. Chem. Acc.*, 2007, **117**, 663; (*b*) X. Q. Gong and A. Selloni, *J. Phys. Chem. B*, 2005, **109**, 19560; (*c*) A. Selloni, *Nat. Mater.*, 2008, **7**, 613.
10 M. kruk and M. Jaroniec, *Chem. Mater.*, 2001, **13**, 3169.
11 (*a*) Y. W. Jun, M. F. Casula, J. H. Sim, S. Y. Kim, J. Cheon and A. P. Alivisatos, *J. Am. Chem. Soc.*, 2003, **125**, 15981; (*b*) J. Polleux, N. Pinna, M. Antonietti, C. Hess, U. Wild, R. Schlogl and M. Niederberger, *Chem.–Eur. J.*, 2005, **11**, 3541.
12 N. G. Park, J. van de Lagemaat and A. J. Frank, *J. Phys. Chem. B*, 2000, **104**, 8989.
13 M. K. Nazeeruddin, A. Kay, I. Rodicio, R. Humphry-Baker, E. Mueller, P. Liska, N. Vlachopoulos and M. Grätzel, *J. Am. Chem. Soc.*, 1993, **115**, 6382.
14 X. Q. Gong, A. Selloni and A. Vittadini, *J. Phys. Chem. B*, 2006, **110**, 2804.
15 (*a*) F. D. Angelis, S. Fantacci, A. Selloni, M. K. Nazeeruddin and M. Gratzel, *J. Am. Chem. Soc.*, 2007, **129**, 14156; (*b*) P. Persson and M. J. Lundqvist, *J. Phys. Chem. B*, 2005, **109**, 11918; (*c*) W. R. Duncan, C. F. Craig and O. V. Prezhdo, *J. Am. Chem. Soc.*, 2007, **129**, 8528.